PROCEEDINGS OF THE ROYAL SOCIETY A

rspa.royalsocietypublishing.org

Research

Article submitted to journal

Subject Areas:
Materials science, Mechanical engineering

Keywords:
Frequency, Fretting wear, Contact geometry, Wear mechanisms

Author for correspondence:
Philip H. Shipway
e-mail: emzphs@nottingham.ac.uk

Fretting wear mapping: The influence of contact geometry and frequency on debris formation and ejection for a steel-on-steel pair

A. R. Warmuth[1], P. H. Shipway[1] and W. Sun[1]

[1] University Technology Centre in Gas Turbine Transmission Systems, The University of Nottingham, Nottingham, NG7 2RD, UK

This paper describes the influence of contact geometry and frequency of oscillation on the formation and ejection of debris from a steel-on-steel fretting contact. Experiments were conducted on specimens in a crossed cylinder on flat configuration for two different conformities, namely a less-conforming and a more-conforming pair, that use a 6 and 160 mm radius cylinder respectively. Both conformities were studied at frequencies from 5 to 200 Hz. It has been found that frequency does not significantly impact the wear behaviour for more-conforming contacts, but does substantial for less-conforming contacts, at high frequency the wear rate is ~50 % of the low frequency experiments. It is proposed that frequency and contact conformity fundamentally influence wear behaviour by control of the type of debris and how it is retained. Debris type (oxidised or metallic) is influenced by frequency which controls the time, and conformity, the distance that atmospheric oxygen has to penetrate the contact. Debris retention is influenced by frequency through the change in temperature, high frequencies result in higher temperatures which encourage debris agglomeration and contact conformity because more conforming contacts become a physical barrier to debris egress. Maps are presented which categorize the observed behaviour and outline a framework by which the basic physical processes can be understood.

Royal Society Publishing
Informing the science of the future

1. Introduction

Fretting is defined as small amplitude oscillatory motion between bodies that are in contact. Fretting wear dominates when a contact is within the *gross sliding* regime, with fretting fatigue dominating in *partial slip* [1]. Gross sliding occurs when the load is small enough and the displacement large enough for the entire contact to be in lateral motion relative to the opposing body (i.e. there are no regions of the contact which are stuck). Fretting wear occurs in many industrial contexts when notionally static contacts (such as bolted or splined connections) experience oscillating loads or vibration. Wear associated with fretting is complex since the damage behaviour is sensitive to a large number of environmental parameters; Dobromirski [2] proposed that there are over 50 parameters which influence fretting behaviour. The damage mechanisms associated with fretting wear are distinct from those associated with sliding wear since the magnitude of movement in fretting is very small in comparison to the size of the contact area, and therefore (for both bodies), most of the contact area remains in contact at all times (referred to as being *covered*); as such, debris development within the contact and its subsequent retention or ejection from the contact greatly influences wear, both in magnitude and mechanism [3]. Work by Ding et al. [4, 5] has argued that the retention of debris can even affect the pressure distribution in the contact, and thus change the development of the shape of the wear scar, and that the debris flow will vary according to position within the contact.

One of the parameters which is known to affect fretting wear behaviour is that of the frequency of oscillation. In some reports in the literature, the selection of frequency has been driven by a desire to directly address the role of this parameter in fretting, or to replicate the conditions of a particular service environment [6, 7]. In other reports, high frequencies have been selected as a means of reducing the testing time [8] (often thereby facilitating the examination of very high numbers of fretting cycles in times that are practicable). However, the actual running of tests at high frequencies is much more experimentally challenging than running tests at lower frequencies; both the mechanical control of motion and the accurate recording of slip and lateral contact forces become more complex as the frequency is increased, and these difficulties have often led to the selection of lower frequencies for experimental test programmes [9]. In light of these issues, the need to understand the role of frequency in the development and mechanisms of fretting wear is required so that experimental results can be compared to one another or related to the industrial context that they may seek to represent.

In this context, it is perhaps not surprising that a significant body of research exists which examines the influence of frequency on fretting wear. The first major studies specifically addressing the role of frequency were communicated by Feng and Uhlig [10] and Uhlig [11], where it was found that the fretting wear rate of a mild steel contact generally decreased as the fretting frequency increased. Tests were conducted over a range of frequencies for a number of different displacement amplitudes and it was found that with higher displacement amplitudes, the influence of frequency was stronger than with smaller displacement amplitudes. This effect of displacement amplitude on the influence of frequency on fretting wear was also confirmed by other research presented in the literature [8, 12, 13].

In the work of Feng and Uhlig [10], it was demonstrated that when fretting tests were conducted in a nitrogen (non-oxidising) atmosphere, the frequency dependency of wear was no longer evident and Uhlig [11] thus proposed that fretting wear is controlled by both chemical and mechanical factors. The chemical factor concerns oxide growth within the contact; when fresh surfaces (generated by asperity shearing due to the fretting motion) are exposed to an oxidising environment, the surfaces oxidise. During subsequent passes, the oxide would be scraped from the surface revealing nascent metal, allowing the oxide growth and removal cycle to repeat. The mechanical factor in fretting wear was described as being due to asperities gouging into the surface and either detaching and adhering, or removing debris from the opposing surface [11]. Oxidation is a time-dependent process, and thus the chemical factor (being controlled by oxide growth on the nascent surfaces) would also be time-dependent; as such (and assuming that the mechanical factors

are time-independent), this role of oxide growth provided an explanation of the role of frequency of oscillation in fretting wear, since changes in the frequency result in changes in the time for oxide growth between consecutive passes of the fretting contact. How this will then influence the contact is complex, as it will depend upon whether the oxide formed is retained in the contact or ejected from it, and whether (if retained) the oxide acts to protect the contact from further wear.

Research by Vaessen et al. [13] also investigated the chemical factor of the frequency effect by removal or limitation of the oxidising environment. This was achieved by running experiments in the following environments; (i) normal air; (ii) nitrogen with 100 p.p.m of oxygen; (iii) silicone oil. Fretting wear experiments conducted in air exhibited a high dependence on the test frequency, with tests conducted at lower frequencies resulting in a higher wear rate (material loss per cycle) than those conducted at higher frequencies. Experiments that were conducted in nitrogen exhibited a much lower dependence of wear rate on frequency (as was found by Feng and Uhlig [10]) and almost no dependence on frequency was observed when tests were conducted in silicone oil. Both research by Feng and Uhlig [10] and Vaessen et al. [13] thus demonstrate that either excluding or reducing the oxidising nature of the environment will reduce the significance of the chemical factor in fretting, and hence reduce the frequency dependence of fretting wear.

In light of the proposal by Uhlig [11] that the time-dependent oxidation process is a key mechanism in the fretting process (and thus explains the frequency effect in fretting), it is unsurprising that the magnitude of the frequency-dependence is also material-dependent (since the oxidation rates and nature of the oxides themselves are well known to be material-dependent). Soderberg et al. [8] reported tests on both carbon steel and stainless steel over a very large frequency range (10 to 20 000 Hz) and found that the wear volume of the stainless steel increased as frequency increased, but that little change was evident for the carbon steel. This observed increase in wear rate with increasing frequency is unique; however, the authors indicated that the wear volumes were approximated from a measure of the wear scar diameter (rather than being a direct measurement of the wear volume), and recognized that the increase in wear volume of the stainless steel may be misleading, as the wear scar diameter (at the higher frequency) was associated with "extensive plastic deformation" rather than just necessarily wear of the contact. However, regardless of the accuracy of measurements of the wear volume, the appearance of the wear scars on the stainless steel samples was clearly more sensitive to fretting frequency than those on the carbon steel samples. It is recognised that whilst changes in material type affect the oxide formation and retention in the contact by changes in oxidation rate, they will also commonly affect it by changes in the mechanics of the contact associated with differences in hardness. Toth [12] argued that softer materials exhibited a high frequency-dependence of fretting wear since metal-metal adhesion was promoted at low frequency, and that adhesion occurred much more readily on softer materials. In addition to these effects associated with gross-sliding fretting, frequency has also been found to influence regime boundaries (in terms of load and stroke) between partial slip and gross sliding in fretting [1, 14, 15].

Laboratory fretting experiments are typically conducted utilising simplified contact geometries. Wear rates derived from such tests are then applied to the modelling of wear in more complex contacts via the use of a time marching finite element analysis (FEA) methodology as developed by McColl et al. [16], which is based upon the assumption that wear rate is independent of the contact geometry itself. More recently, this assumption has been cast into doubt. Fouvry et al. [7] and Merhej and Fouvry [17] found that for simplified contacts (ball-on-flat and cylinder-on-flat), the wear rate decreased as the radius of curvature of the non-plane body increased. They proposed that this decrease in wear was due to the restriction of debris ejection from the contact associated with a curved body with higher radius, with the entrapped debris protecting the contact from further wear. Warmuth et al. [18] made similar observations (again with a cylinder-on-flat contact geometry) and sought to present microstructural evidence to explain this effect. They argued that the reduction in wear rate with increasing radius is due to a change in wear mechanism. In a less-conforming contact (smaller cylinder radius), oxygen was able to penetrate the contact easily, facilitating the formation of oxide wear debris which then flowed out of the contact. In

Table 1: Chemical composition of the high strength steel (wt%) [21].

C	Si	Mn	P	S
0.35-0.43	0.1-0.35	0.4-0.7	<0.007	<0.002
Mo	Ni	V	Fe	Cr
0.8-1.10	<0.3	0.15-0.25	Remainder	3.0-6.35

contrast, as the contact became more-conforming (larger cylinder radius), oxygen was effectively excluded from the centre of the contact, resulting in metal-metal adhesion and metal transfer between the contact faces; at high fretting displacement amplitudes, this transfer was significant and the formation of substantial pits and peaks within the contact (with features measuring up to 140 µm deep) was observed. Fouvry and Merhej [19] also found that for large radius specimens (i.e. a more conforming contact), a metallic region in the centre of their contact developed and this was also attributed to being due to oxygen exclusion.

Van Peteghem et al. [6] examined the fretting of a titanium alloy contact as a function of frequency at very low frequencies (between 0.11 to 5 Hz) on a reasonably conforming cylinder-on-flat contact (80 mm radius cylinder). Under a constant load, wear at low frequency was observed to be more than five times higher than that observed at the higher frequency. At both frequencies, the debris at the centre of the contact was dominated by titanium nitride rather than titanium oxide, with the latter being the primary debris surrounding the very outer region of the contact. The formation of titanium nitride indicated that the area of the contact was depleted in oxygen, indicating that ingress of the atmosphere into the contact is a critical process in the development of fretting damage (Mary et al. [20]). Addressing the frequency effect, Van Peteghem et al. [6] argued that a decrease in fretting frequency would decrease the frictional power dissipated in the contact, and thus the temperature of the contact would also fall. They argued that this implies that the increase in wear rate with decreasing frequency cannot therefore be linked to the kinetics of the process of oxide formation itself (since the oxidation kinetics will decrease with decreasing temperature). Accordingly, they suggested that "increasing the time that oxygen can react with the native titanium metal" (associated with the increase in time between asperity contacts as the frequency is reduced) is the primary mechanism by which the increase in wear rate with decreasing frequency is best explained.

From the literature, it is thus clear that mechanisms and rates of fretting wear depend upon the formation of oxide in the contact, and its retention in or ejection from the contact. Moreover, it is clear that both fretting frequency and contact conformity influence these. In order to better understand the roles of debris formation, retention and ejection in fretting, the work here seeks to provide a detailed study where both fretting frequency and contact conformity are varied, facilitating the development of a coherent understanding of the role of debris in fretting.

2. Experimental procedure

(a) Specimen, test procedure and conditions

Fretting wear experiments were conducted on high strength steel specimens; the chemical composition of this steel is detailed in Table 1. The heat treatment of the steel was performed prior to machining to size (the details of this heat treatment process can be found elsewhere [21]) and resulted in the specimens having a hardness (HV_{20}) of 465–480 kgf mm^{-2}.

The specimen pair was assembled in a cylinder-on-flat configuration, as shown in Fig. 1. The flat and cylindrical specimens were ground on a linear and cylindrical grinder respectively, with cylindrical specimens being manufactured with radii of both 6 mm and 160 mm. The flat and cylindrical specimens had a roughness (Ra) of 0.1 to 0.3 µm and 0.4 to 0.7 µm respectively. The

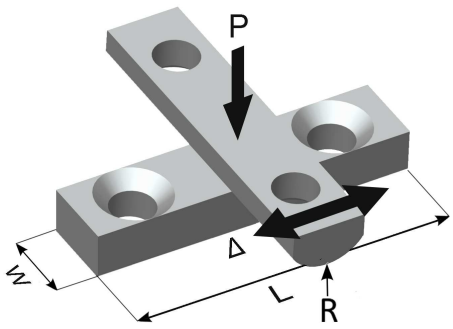

Figure 1: Crossed cylinder-on-flat specimen configuration utilised in fretting tests.

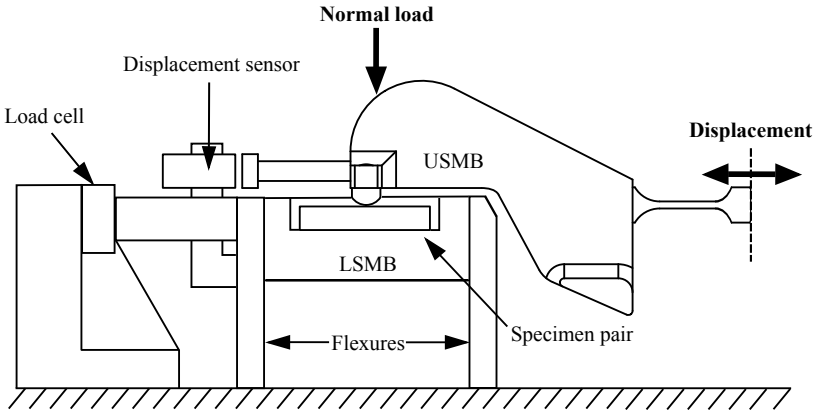

Figure 2: Illustration of the main components of the fretting apparatus used in this study.

flat specimen is mounted on the lower specimen mounting block (LSMB) which is stationary and the cylindrical specimen is mounted on the upper specimen mounting block (USMB). The USMB was loaded through a dead weight configuration and the normal load that results is termed P. The main components in the rig used for the fretting experiments are illustrated in Fig. 2. The motion of the USMB (and hence the cylindrical specimen) is created by a force generated by an electromagnetic vibrator (EMV). The displacement, Δ, of the USMB is monitored by a capacitance displacement sensor which is mounted to the LSMB and is recorded throughout the length of the test. The amplitude of the force input is controlled to achieve a set displacement amplitude, Δ^*, for the test.

The lateral force, Q, is measured and recorded throughout the entire test by a piezoelectric load cell which is connected to the quasi-stationary LSMB. The LSMB is mounted on flexures which provide flexibility in the horizontal direction so that the majority of the lateral force is transmitted though the much stiffer load path which contains the load cell as shown in Fig. 2. Both displacement and load sensors have been calibrated (both externally and in-situ) in static conditions. The load and displacement signals are sampled at a rate of two hundred measurements per fretting cycle at all fretting frequencies.

The behaviour of the contact can be monitored throughout the test by examination of the fretting loops; a fretting loop is a plot of a cycle of the measured lateral force as a function of the displacement. In gross sliding, the entire contact is in relative tangential motion with respect to the opposing contact face; this regime was maintained throughout the test by ensuring that the load conditions were chosen so that the fretting loop exhibited a quadrilateral shape; an ideal

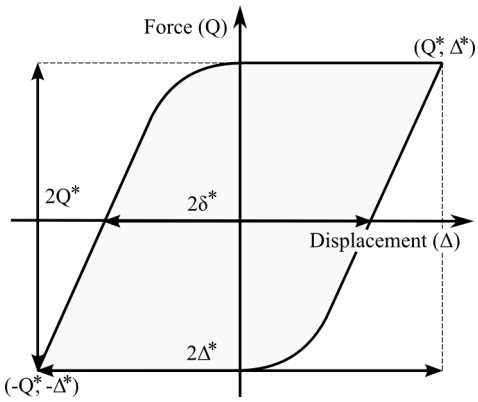

Figure 3: Schematic diagram of an ideal fretting loop in the gross sliding regime, illustrating parameters defined in the text.

Table 2: Summary of the fretting test parameters.

Normal load	250 N
Displacement amplitude	50 µm
Cylinder radii	6 and 160 mm
Test duration	100 000 cycles
Oscillation frequencies	5, 20, 100 and 200 Hz

gross-slip loop is plotted in Fig. 3. The displacement of the USMB is measured, but it must be noted that this is not the same as the slip in the contact; there are components with compliance which physically separate the contact from the point of measurement, and hence the measured displacement amplitude is always slightly larger than the contact slip amplitude, δ^*. One of the critical reasons for recording a fretting loop is that the actual contact slip amplitude (δ^*) can be derived by measuring the distance from the origin to the displacement measured at zero force, as seen in Fig. 3. Traditionally, the coefficient of friction is found by dividing the frictional force measured at the maximum displacement amplitude by the applied normal load. However, Fouvry et al. [22] proposed that significant changes were often observed in the lateral force throughout the sliding part of the fretting loop, and that instead, the energy dissipated per cycle (i.e. the area of the fretting loop) could be utilised to generate a friction coefficient more representative of the overall behaviour of the contact. Thus, for these experiments, the energy coefficient of friction (ECOF) as proposed by Fouvry et al. has been used; this parameter is calculated as shown in Eq. (2.1), where E_d is the dissipated energy per cycle.

$$ECOF = \frac{E_d}{4\delta^* P} \tag{2.1}$$

Tests were conducted on less-conforming contact pairs (which used cylinders with a radius, R, of 6 mm) and more-conforming contact pairs (which used cylinders with a 160 mm radius). The flat specimen has a width, w, of 10 mm as seen in Fig. 1 (this defines the contact length). Experiments were conducted under a normal load of 250 N and an applied displacement amplitude, Δ^*, of 50 µm. The far-field surface temperature of each specimen was measured via a thermocouple that was spot welded to specimen surfaces on the centreline and at a distance of approximately 10 mm from the fretting contact. Tests were conducted in an ambient environment with a temperature of 23 °C and a relative humidity of 32 % typical of all the tests. Experiments were conducted at frequencies of 5, 20, 100 and 200 Hz for a duration of 100 000 cycles; the test information is summarized in Table 2.

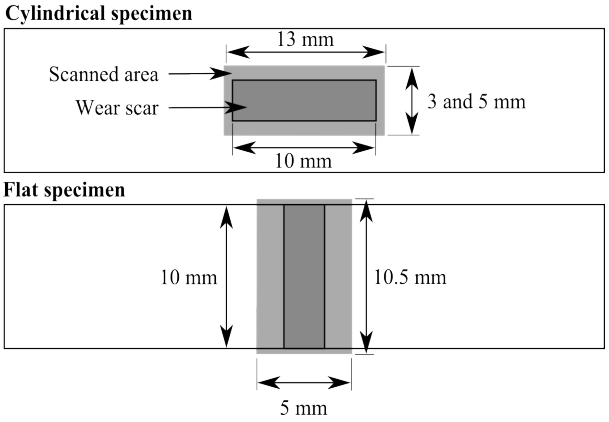

Figure 4: Illustration of the areas profiled on both the flat and cylindrical fretting specimens.

(b) Estimation of wear volume and surface topography

After the completion of a fretting experiment, the specimens were lightly swabbed with industrial methylated spirit to remove loose debris, thus leaving any debris that was adhered to the specimen. To evaluate their topography, the wear scars on both the flat and cylindrical specimens were scanned using a Bruker Contour GT-I interferometer, which has a vertical resolution of $\sim$0.15 nm and a lateral resolution of 4 µm. The scan area on the flat specimen was 5 mm in width and 10.5 mm in length; scans on the cylindrical specimen were 3 mm in width for the less-conforming scars and 5 mm for the more-conforming wear scars, both having a scan length of 13 mm as represented in Fig. 4. Scans on the cylindrical specimen extended outside the wear scar so that the unworn surface could be used to create (by interpolation) a reference surface (representing the surface before wear occurred), as proposed by Elleuch and Fouvry [23] and illustrated in Fig. 5. The volume below each reference surface was regarded as the wear volume (V^-_{Flat} and V^-_{Cyl} for the flat and cylindrical specimens respectively) and the volume of material above these surfaces was regarded as transferred volume (V^+_{Flat} and V^+_{Cyl} for the flat and cylindrical specimens respectively). The total wear and transfer volumes for the couple (V^- and V^+ respectively) are defined as the sum of the respective volumes for the flat and cylindrical specimens. Wear and transfer rates for the contact pair were calculated based on the displacement amplitude (δ^*) and the number of cycles per test (C), as indicated in Eq. (2.2) and Eq. (2.3)

$$\dot{V}^- = \frac{V^-}{4\delta^* PC} \tag{2.2}$$

$$\dot{V}^+ = \frac{V^+}{4\delta^* PC} \tag{2.3}$$

(c) Characterization of wear scars and debris

Scanning electron microscopy was used to characterise the nature of the wear scars, using a Philips XL30 scanning electron microscope. Backscattered electron (BSE) images were used to distinguish oxide from metallic material, as oxide which forms in the wear scar has a lower average atomic number, resulting in a lower brightness in BSE imaging than the steel. The identification of oxide was confirmed qualitatively by energy-dispersive x-ray (EDX) analysis (although this technique is not able to produce a quantitative analysis due to the low energy of the X-rays associated with oxygen and the low thickness of the oxide beds being examined). Cross-sections through the specimens were used to investigate the structure of the debris beds as well as to reveal any subsurface damage. Sections were taken from the cylindrical specimen (through an area of interest

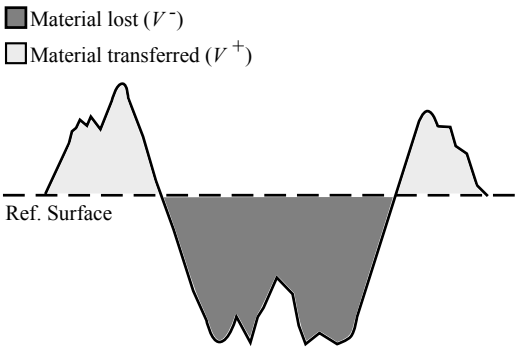

Figure 5: Illustration of the definition of wear and transfer volumes in a fretting scar.

identified by top surface BSE images or profilometry) and then mounted in a conductive phenolic mounting resin. Once mounted, specimens were ground with silicon carbide paper and then polished with 6 µm and then 1 µm diamond paste. To reveal microstructural features in the cross-sections, specimens were etched with 5 % nital. The powdered debris that was ejected from the contact was collected from the flat specimen and analysed by X-ray diffraction (XRD) using a Siemens D500 powder diffractometer with Cu−Kα radiation.

3. Experimental results

(a) Effect of frequency on less-conforming contacts

Fretting wear experiments were conducted with 6 mm radius cylinders at frequencies of 5, 20, 100 and 200 Hz. The surface topographies of the wear scars for the flat and cylindrical specimens worn at these frequencies are presented in Fig. 6; the form from the cylindrical specimens has been removed so that damage resulting from the fretting test can be better compared to that observed on the flat specimens. As can be seen from the surface topographies, the wear scars resulting from tests conducted over the range of frequencies are all of similar width ($\sim$1 mm). The fretting wear scar on the flat specimen from the 5 Hz test is *Vee* shaped and has an average maximum depth of 15 µm; for higher frequency tests, the bottom of the equivalent wear scar flattens and becomes much shallower, exhibiting an average maximum depth of 6.6 µm for the test conducted at 200 Hz.

Plots of rates of wear and transfer as a function of fretting frequency are presented in Fig. 7a. For the tests conducted at 5 and 20 Hz, the wear rate is large (similar values of around 4.6×10^{-5} to 5.3×10^{-5} mm^3 N^{-1}m^{-1}); as the frequency was increased, the wear rate decreased, with the wear rate at 200 Hz being $\sim$50 % of that recorded at the lower frequencies.

In Fig. 7b, the increases in temperature above ambient recorded by the thermocouple on the cylindrical specimen during the fretting tests are presented (the thermocouple is positioned far from the fretting contact as described in Section (a)). The temperature changes associated with the tests conducted at 5 and 20 Hz are both very small, being less than 1 °C and 3 °C respectively. In contrast, the temperature increased very rapidly at the beginning of the test for both the 100 and 200 Hz tests, tending towards steady state values of increased temperature of approximately 12.5 °C and 20.5 °C respectively.

Fig. 8a are fretting loops for the tests conducted at different frequencies. The 5 Hz fretting loop is quadrilateral in shape, much like the *ideal* fretting loop illustrated in Fig. 3. However, at the higher fretting frequencies (100 and 200 Hz), the top and bottom of the fretting loop exhibit some limited waviness, probably associated with system vibration at these higher frequencies.

In Fig. 8b, traces showing the development of the ECOF with the number of fretting cycles are presented for the different frequencies examined. The 5 Hz test has a pronounced initial rise at the beginning of the test to a maximum of 0.84 which then gradually reduced toward a steady state value of 0.7. At 20 Hz, the ECOF rises to 0.81 and then reduces to a steady state of 0.77. The 100 Hz test rose to a maximum and steady state value of 0.76 which is slightly higher than the steady state value observed in the 5 Hz experiment. At 200 Hz, the ECOF rises much like that in the 100 Hz test, and settles at a slightly smaller value of approximately 0.7.

Fig. 9 presents images of the flat specimens following fretting tests at both 5 and 20 Hz, with the images being taken immediately following the removal of the USMB. In both cases, substantial amounts of loose dark brown debris are piled up on both of the edges of the fretting wear scar, with the volume of debris being clearly larger for the test conducted at 5 Hz. The debris has been analysed by XRD which indicates that the debris is primary composed of Fe_2O_3 and a small amount of unoxidised metal.

BSE images of the fretting wear scars on the flat specimens from tests conducted across the range of fretting frequencies are shown in Figs. 10a to 10d (low magnification) and Figs. 10e to 10h (high magnification). As can be seen in Figs. 10a and 10e, the surface of the 5 Hz wear scar is primarily metallic (regions of bright contrast) with small amounts of oxidised debris (dark in contrast) on the outside edge of the wear scar. The bright areas and dark areas on the wear scar were confirmed as being primarily metal and oxide respectively through the use of qualitative EDX analysis. Figs. 10b to 10d and Figs. 10f to 10h show the surfaces of the wear scars resulting from fretting at 20, 100 and 200 Hz and it is seen that in each case, the surfaces are covered with dark oxidised debris over nearly the entire scar, with only small patches of metallic surface being visible. In each case, EDX analysis was used to verify that the dark regions in the scars were primarily oxide.

Fig. 10i is high magnification BSE image of a cross section through the 5 Hz fretting wear scar on the cylindrical specimen; this shows that the surface consists of deformed metallic regions alongside regions covered with an oxide layer of $\sim$1 µm in thickness. A corresponding cross section through the scar formed on the cylindrical specimen by fretting at 200 Hz is presented in Fig. 10j. Here, a much thicker debris bed is present on the surface ($\sim$3 µm in thickness) but small bright regions within the layer indicate that whilst the debris is primarily oxide, some metallic particles are embedded within it.

(b) Effect of frequency on more-conforming contacts

The influence of fretting frequency was also studied for more-conforming contacts, with testing taking place with cylinders that have a radius of 160 mm. The surface profiles of the wear scars from the flat and cylindrical specimen fretting are presented in Fig. 11. The surface of the flat specimen following testing at 5 Hz exhibits only small amounts of wear; the scar is complete across the entire width of the specimen and although it is not very deep, it is around 3 mm in width (much wider than the equivalent scars associated with the less-conforming contacts). The surface of the specimen following a test at 20 Hz exhibits more peaks and pits than observed on the flat specimen following a 5 Hz test. The surfaces of the specimens following tests at fretting frequencies of 100 and 200 Hz exhibit significant pitting, which is observed to occur towards the centre of the contacts. At all the higher fretting frequencies, the scar does not reach the edges of the specimen as it did following the 5 Hz test.

Fig. 12a presents plots of the wear and transfer rates for the fretting tests conducted with the more-conforming contacts. The wear rates associated with the more-conforming contacts are much lower than the rates for the tests conducted with the less-conforming contacts (Fig. 7a), and are not as strongly influenced by the fretting frequency. A similar effect was observed by Vaessen et al. [13], where they observed the wear rate (per cycle) decreasing with increasing fretting frequency in normal atmospheric conditions, but also that the effect of frequency on wear rate became much less significant in environments where oxidation was restricted (in their case, by the use of an almost oxygen-free atmosphere). The similarity between the observations of Vaessen et al. [13]

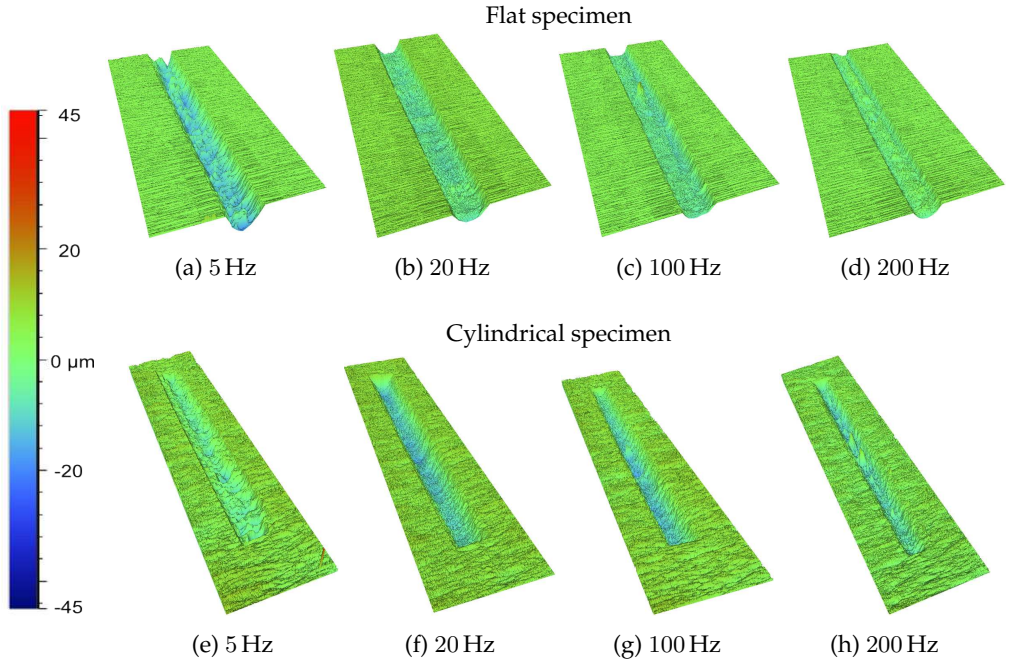

Figure 6: Surface profiles of the fretting wear scars on both the flat and cylindrical specimens for fretting tests conducted at frequencies of 5, 20, 100 and 200 Hz with 6 mm radius cylindrical specimens.

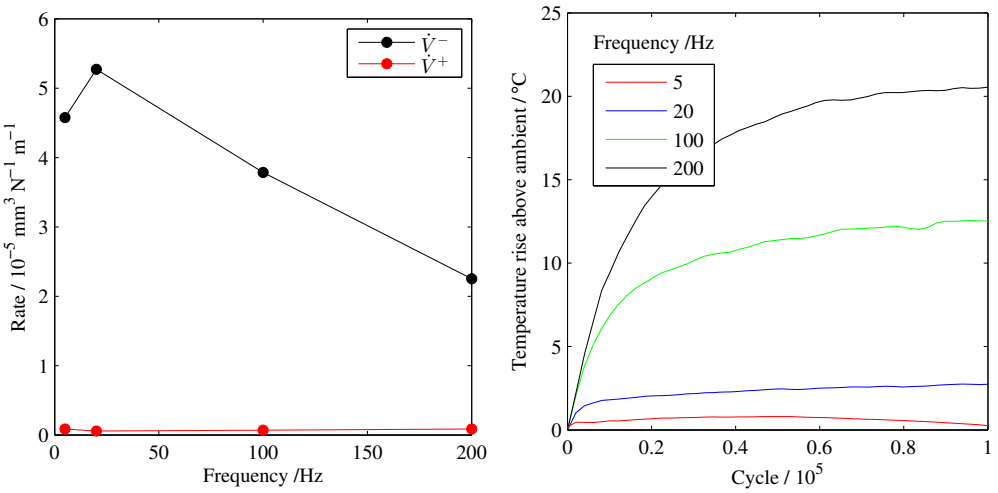

(a) Wear rates (b) Temperature change

Figure 7: (a) Plot of wear rate ($\dot{V}^-$) and transfer rate ($\dot{V}^+$) and (b) measured specimen far-field temperature rise above ambient for fretting wear tests conducted with 6 mm cylindrical specimens at test frequencies of 5, 20, 100 and 200 Hz.

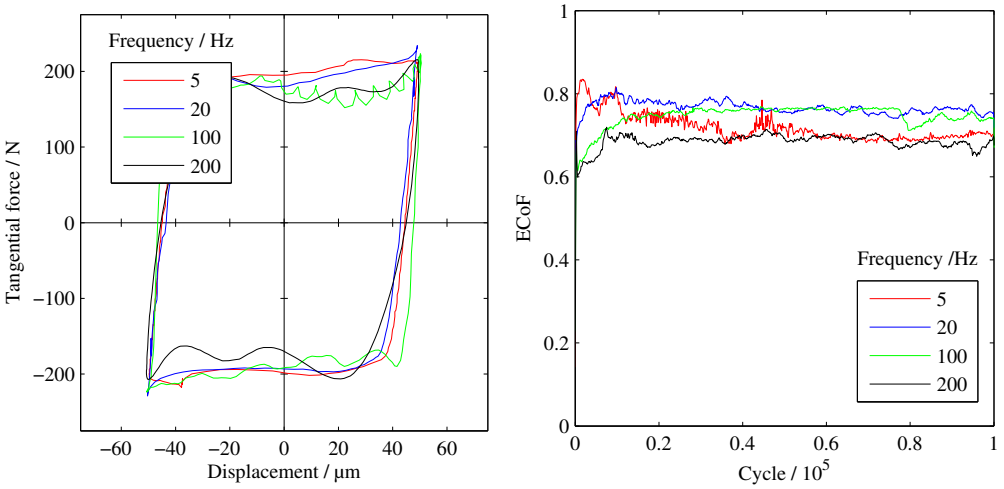

(a) Fretting loops (b) Energy based coefficient of friction

Figure 8: (a) Fretting loops and (b) plots of development of ECOF with number of fretting cycles for fretting wear tests conducted with 6 mm cylindrical specimens at test frequencies of 5, 20, 100 and 200 Hz.

(a) 5 Hz (b) 200 Hz

Figure 9: Images of debris surrounding the fretting wear scars on the flat specimens immediately following removal of the USMB. Fretting tests performed with 6 mm radius cylindrical samples at (a) 5 Hz and (b) 200 Hz.

and those presented in this work lend weight to the hypothesis that the more-conforming contact geometry restricts ingress of atmospheric oxygen to the central regions of such contacts.

In contrast to the wear rates, Fig. 12a indicates that the transfer rates with more-conforming contacts are much greater than those observed with the less-conforming contacts; indeed, it can be seen in Fig. 12a that the wear and transfer rates are of similar magnitude, implying that wear debris is not leaving the contact as readily. In comparing the wear and transfer rates, it must be remembered that there is a natural volume expansion when steel reacts to form an oxide debris, since both Fe_2O_3 and Fe_3O_4 have a Pilling-Bedworth ratios of greater than two [24].

The increase in specimen far-field temperature above ambient over the test duration for the experiments with more-conforming contacts are presented in Fig. 12b. Again, the temperature increase above ambient for the experiment run at 5 Hz was very small, with an increase of only $\sim$1 °C by the end of the test. In contrast, the temperature increased very rapidly at the beginning

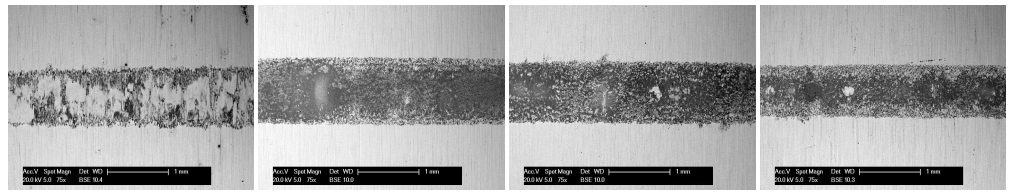

(a) 5 Hz (b) 20 Hz (c) 100 Hz (d) 200 Hz

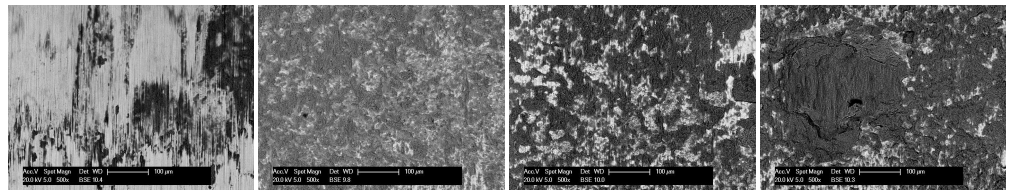

(e) 5 Hz (f) 20 Hz (g) 100 Hz (h) 200 Hz

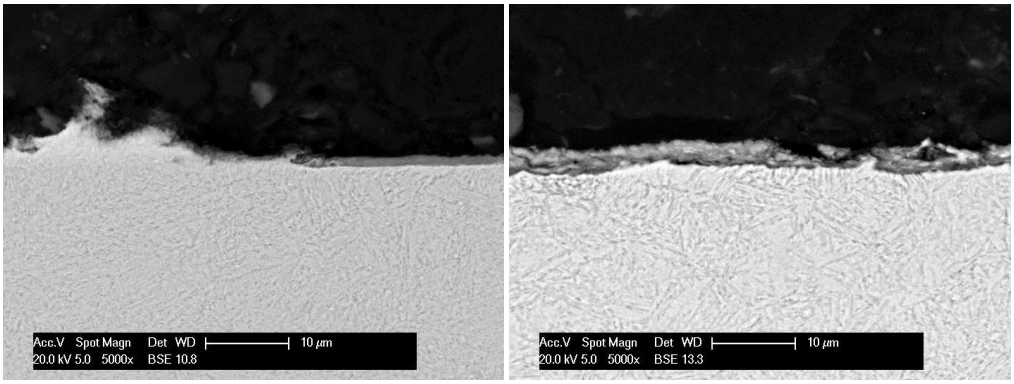

(i) 5 Hz (j) 200 Hz

Figure 10: BSE images of fretting wear scars at low and high magnification following experiments conducted with 6 mm cylindrical specimens at the frequencies indicated. (a) - (h) are top surface images of wear scars on the flat specimens; (i) and (j) show cross-sections through the scars on the cylindrical specimens.

of the test for both the 100 and 200 Hz tests, tending towards steady state values of increase in temperature above ambient of approximately 10.0 and 28.5 °C respectively.

Fretting loops for the tests conducted at different frequencies for the more-conforming contacts are presented in Fig. 13a and are very similar to the fretting loops associated with the less-conforming tests (Fig. 8a). The 5 Hz fretting loop is stable, but for the tests conducted at higher frequencies, the loop top/bottom again exhibits some instability.

Traces describing the development of ECOF with the number of fretting cycles as a function of fretting frequency are shown in Fig. 13b. The ECOF for the 5 Hz test reaches a maximum of 0.83 very early in the test which then steadily decreases until reaching a value of 0.66. The test conducted at 20 Hz exhibited a lower initial value of ECOF which then rose to a steady value of around 0.74. The development of ECOF for tests conducted at both 100 and 200 Hz are very similar, both exhibiting high initial values which first decreased rapidly, and then increased throughout the test before stabilizing at approximately the same ECOF as that observed in the 5 Hz test.

BSE images of the fretting wear scars on the flat specimens from tests conducted with the more-conforming cylinder geometry across the range of fretting frequencies are shown in Figs. 14a

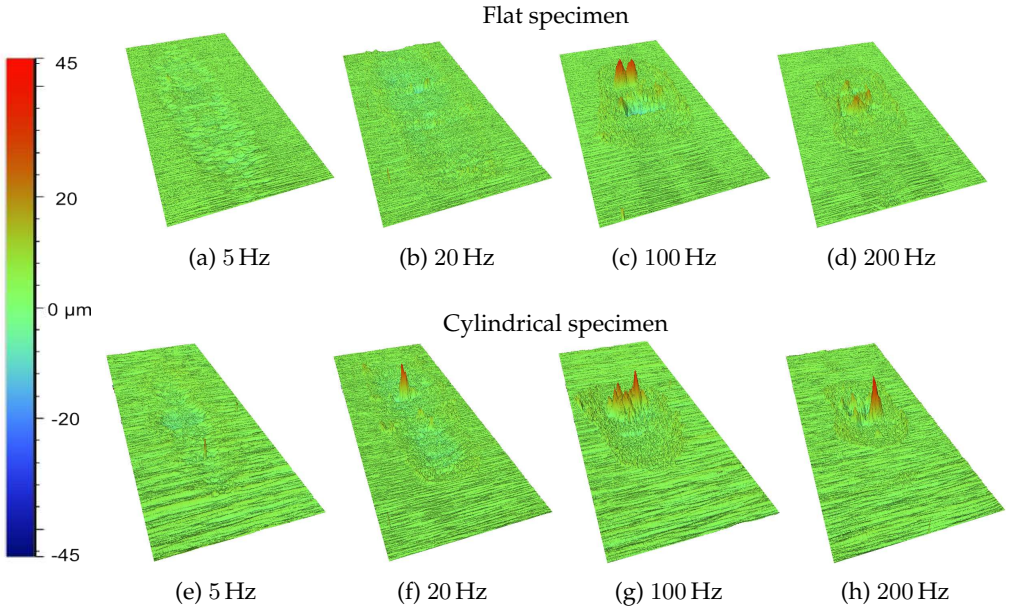

Figure 11: Surface profiles of the fretting wear scars on both the flat and cylindrical specimens for fretting tests conducted at frequencies of 5, 20, 100 and 200 Hz with 160 mm radius cylindrical specimens.

to 14d (low magnification) and Figs. 14e to 14h (high magnification). Fig. 14a is an image of the specimen following a test at 5 Hz and it is seen that there are dark patches of oxidised debris in the centre of the wear scar, as was observed on the less-conforming contacts; qualitative EDX analysis has been used to confirm that this dark region was oxidised debris, with the outer region of the scar being found to be primarily metallic. Fig. 14b is an image of the specimen following a 20 Hz test and shows that nearly all of the surface is covered with adhered oxide. Fig. 14c and Fig. 14d show the worn surfaces of the specimens from the 100 and 200 Hz tests; in both cases, the wear surface exhibits a dark contrast, associated with being covered by an oxide debris. The scar resulting from the test at 200 Hz (Fig. 14d) is smaller than the scar that was produced by fretting at 100 Hz, but the trend is very similar, with both contacts being mainly covered in oxide debris with a light region in the centre of each scar (qualitative EDX indicates that dark areas are indeed oxide).

Fig. 14i is a high magnification BSE image of a cross-section through a 160 mm cylindrical specimen following fretting at 5 Hz; the figure is a composite image, showing the centre of the fretting wear scar (which can be seen to be composed primarily of oxide debris) and the periphery of the contact where the presence of metallic debris dominates. Fig. 14j is a high magnification BSE image of the centre region of the scar from the 200 Hz experiment; it is clear that in this case, the debris bed is very different to those observed earlier, being $\sim$10 μm thick and being comprised primarily of large metallic particles.

4. Discussion

(a) Less-conforming contacts

It is clear from the experimental results that test frequency exerts a strong influence on the fretting wear behaviour of steel-on-steel contacts; however, in the case of the more-conforming contacts, this influence is not observed via the wear rate, but only through the nature of the wear debris. For less-conforming (6 mm cylindrical radius) contacts, increasing the frequency from 5 to 200 Hz

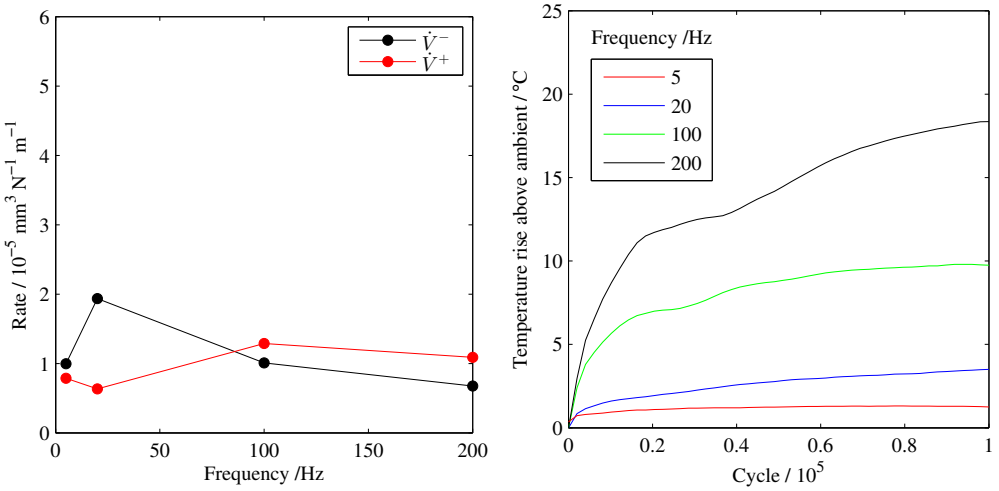

(a) Wear rates (b) Temperature change

Figure 12: (a) Plot of wear rate ($\dot{V}^-$) and transfer rate ($\dot{V}^+$) and (b) measured specimen far-field temperature rise above ambient for fretting wear tests conducted with 160 mm cylindrical specimens at test frequencies of 5, 20, 100 and 200 Hz.

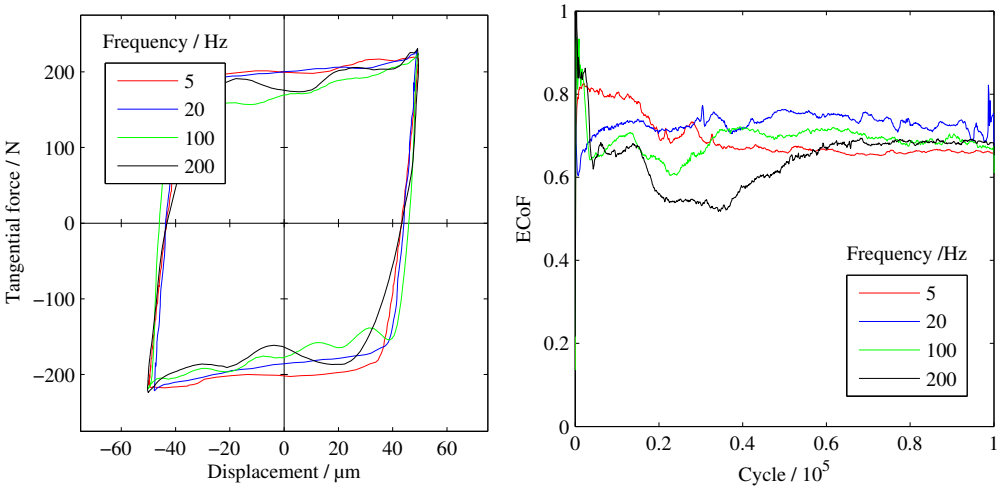

(a) Fretting loops (b) Energy based coefficient of friction

Figure 13: (a) Fretting loops and (b) plots of development of ECOF with number of fretting cycles for fretting wear tests conducted with 160 mm cylindrical specimens at test frequencies of 5, 20, 100 and 200 Hz.

results in an ∼50 % reduction in wear rate (Fig. 7a). The ECOF plots for all the frequencies examined for the less-conforming contacts (Fig. 8b) are high, exhibiting an average steady state value of ∼0.73; these values are very similar despite the differences in the observed rates of wear (Fig. 7a). This influence on the wear rate is also evident upon observation of the surface profiles of the wear scars (Fig. 6), where at low fretting frequencies, the surface of the wear scar is deep, heavily gouged

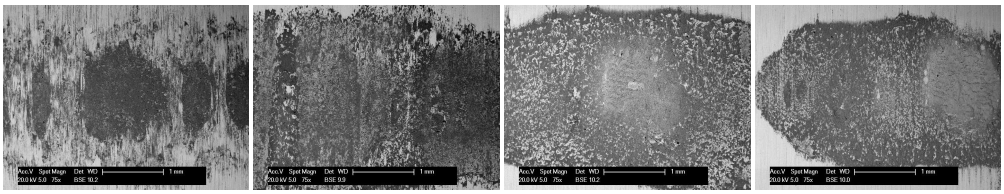

(a) 5 Hz (b) 20 Hz (c) 100 Hz (d) 200 Hz

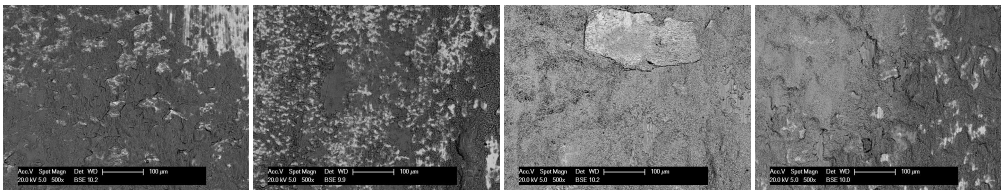

(e) 5 Hz (f) 20 Hz (g) 100 Hz (h) 200 Hz

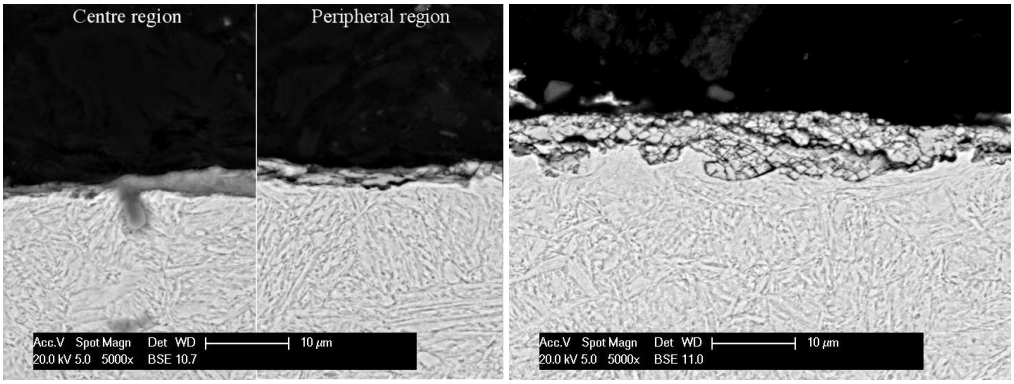

(i) 5 Hz (j) 200 Hz

Figure 14: BSE images of fretting wear scars at low and high magnification following experiments conducted with 160 mm cylindrical specimens at the frequencies indicated. (a) - (h) are top surface images of wear scars on the flat specimens; (i) and (j) show cross-sections through the scars on the cylindrical specimens.

and *Vee* shaped, whereas at higher frequencies, the wear scars are less deep and have a more finely roughened surface.

BSE images of the flat specimen wear scars for the different frequencies examined (Figs. 10a to 10d) indicate that at 5 Hz, the wear scar surface is primarily metallic, but at higher frequencies, the wear scar is characterised by the presence of an oxide debris bed. However, Fig. 9a indicates that oxide is readily forming during fretting at 5 Hz, and thus we may conclude that at this frequency, it is not the ability to form the oxide, but instead the ability to retain the oxide debris in the contact during fretting that differs from that at the other fretting frequencies. At higher frequencies, there is more frictional power being dissipated into the contact and, as a result, the contact temperature will be significantly increased (the effect of this is observed even in far-field temperature measurements as seen in Fig. 7b). Schouterden et al. [25] have previously reported a similar effect, in that at lower fretting frequencies, debris was observed to be ejected from the contact but that at higher frequencies, they argued that due to the increase in frictional power dissipation, an adhered debris bed was developed and maintained which reduced the observed wear rate. Thus, we see that for the less-conforming contacts, oxide debris is being formed within the contact at all frequencies

examined; at lower frequencies, this debris is ejected form the contact, but at higher frequencies, the debris adheres to the contact surface as a result of the increase in temperature in the contact, and its retention in the contact results in a reduction in wear.

The retention of debris within the contact as the contact temperature increases may result from sintering of the debris (such sintering of debris has been observed during fretting at 20 Hz upon increasing the ambient temperature from room temperature to just 85 °C [26]), or from softening of the substrate which will promote debris keying into the surface. Pearson et al. [26] have argued that debris created in a fretting contact may have many unique attributes that enable it to sinter at very low temperatures; one of these is that the oxide particles created are very small (commonly < 5 nm [27]) and that very rapid rates of sintering are observed with such small particles [28]. As debris begins to sinter, its egress from the contact will be influenced. The flow of debris out of the contact has been modelled by Leonard et al. [29]; in this study, debris is modelled as discrete elements with spring and damper connections, allowing the formation of platelets to be mimicked. Platelets are thin debris features that are composed of sintered or adhered debris, as experimentally observed by Soderberg et al. [8]. The modelling suggests that as the platelet features became longer, they interlock and form a thicker third-body layer. Therefore, it is suggested that even small amounts of debris sintering can lead to debris entrapment within the contact as this model has indicated.

Whilst it has thus been argued that debris retention is affected by the temperature in the contact (which depends in turn upon the fretting frequency), it is clear that changes in fretting frequency will also affect other processes related to the formation of the oxide debris. The increase in contact temperature associated with increasing frequency will *enhance* the kinetics of oxide formation; however, the increase in frequency will also *reduce* the time between asperity interactions in the contact, which will serve to limit oxidation. As such, changes in frequency may be expected to lead to changes in the nature of the debris, but given the competing effects, it is not possible to predict what the changes will be. The work of Van Peteghem et al. [6] suggested that the increased time between asperity contacts as the frequency is reduced is the primary mechanism by which the increase in wear rate with decreasing frequency is best explained.

In this regard, there is some evidence in the work on the less-conforming contacts that there is a subtle change in the nature of the debris. In all cases, the debris is primarily oxide; however, where debris is observed on the surface of contacts fretted at low frequency (Fig. 10i), only oxide is observed, whereas in the debris layer on the contact fretted at 200 Hz, there is some evidence of metallic particles being present in the primarily oxide debris bed (Fig. 10j). This presence of metallic particles in the debris indicates that in this case, the reduction in time between asperity contacts associated with the increase in fretting frequency is the dominating effect.

(b) More-conforming contacts

As found in previous research in the area [7, 17–19], wear during fretting of more-conforming contacts (tests utilising 160 mm radius cylindrical specimens) is found to be much lower than that observed in less-conforming contacts at all fretting frequencies examined. The results for tests with the more-conforming contacts (Fig. 12a) show that as the fretting frequency is increased, the wear rate reduces only slightly. As observed for fretting with the less-conforming contacts, the steady state ECOF was very similar for all frequencies examined, having an average steady state ECOF of $\sim$0.7; however, much wider variation in ECOF was observed in the early stages of these tests than was observed for the less-conforming contacts. Investigation of the surface profiles of the fretting wear scars (Fig. 11) indicates that at low frequencies, the wear scar extended across the entire width of the contact but that at higher fretting frequencies, the wear scar was isolated towards the centre of the contact and only small amounts of damage occurred across the width of the scar.

From the BSE images of the wear scars on the flat specimens following fretting (Figs. 14a to 14d), it is clear that the wear behaviour associated with more-conforming contacts is quite different to that observed in tests conducted with the less-conforming contacts. There are two regions within the contact that exhibit very different wear behaviour, namely a central region and a peripheral region. At low fretting frequencies, the peripheral region (which is closest to the exit of the contact)

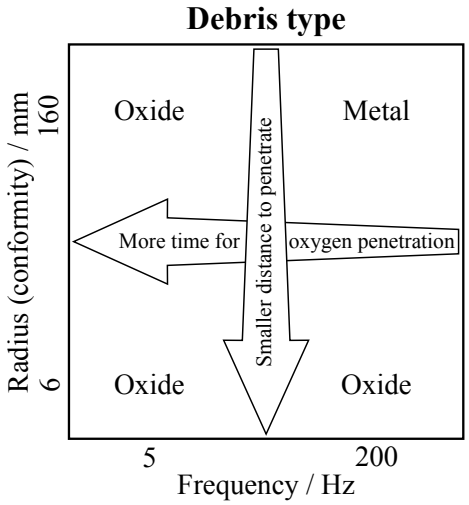

Figure 15: Debris type fretting map, identifying the nature of the debris formed during fretting as a function of contact conformity and fretting frequency. Superimposed on the map are arrows representing changes in fundamental processes associated with oxygen penetration into the contact which depend upon the parameters upon which the map is constructed.

experiences high wear, and the wear scar surface is primarily metallic (with low levels of oxide coverage), much like that observed following low frequency fretting of the less-conforming contact. At higher frequencies, the peripheral region becomes covered in adhered oxidised debris, again, much like the observations made of the wear scars associated with the less-conforming contacts. As such, the periphery of the more-conforming contact exhibits very similar behaviour to that of whole scar from a less-conforming contact across the range of fretting frequencies examined, with this being explained by similarity of these two regions in terms of ease of access of environmental oxygen into the contact, and in terms of ease of egress of the fretting debris from the contact.

In contrast, the wear behaviour of the central region of the scar on the more-conforming contact is very different. At low frequencies, the central region of the scar is primarily covered with oxide debris but at higher fretting frequencies, this region was much lighter in contrast when observed under BSE imaging, indicating that the wear debris is primarily metallic in nature. Cross-sections through the fretting wear scars on the cylindrical specimens confirm that the debris in the central region following fretting at low frequencies (5 Hz) is primarily oxide whilst the peripheral region exhibits a metallic surface (Fig. 14i). However, with fretting frequencies of 200 Hz, the central region of the scar is primarily composed of fine metallic debris (Fig. 14j), with the adhered bed being $\sim$5 µm thick. This metallic debris indicates that under these conditions, environmental oxygen is not able to penetrate the contact at a rate sufficient to promote the formation of normal oxide debris (at this high frequency, the frictional power dissipated is high, resulting in a high contact temperature, so it can be postulated that it is the limited oxygen supply, rather than the slow oxidation kinetics which is limiting the formation of oxide). However, the fact that a predominantly oxide debris bed is formed (i) under this contact geometry when fretted at lower frequencies (e.g. Fig. 14i) and (ii) at this high frequency with a less-conforming contact (Fig. 10j) indicates that effective oxygen exclusion from this contact results from the combination of the high fretting frequency (with its reduced time between individual asperity contacts in the wearing zone) and the more-conforming geometry (which results in physical exclusion of atmospheric oxygen from the contact associated with the extended distances over which the oxygen has to penetrate). Similar conclusions have been drawn by Van Peteghem et al. [6] based upon experiments on fretting of titanium contacts, where the presence of titanium nitride as the debris in the central region of a

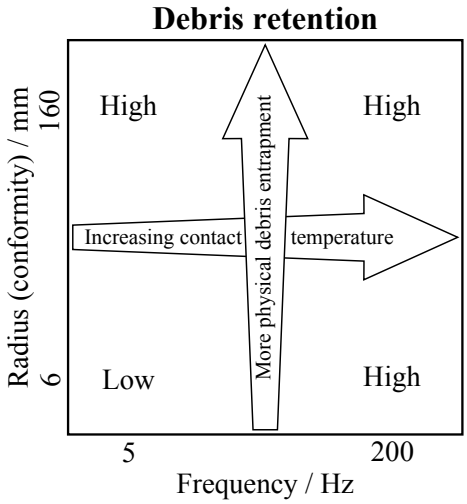

Figure 16: Debris retention fretting map, identifying the propensity for the debris formed during fretting to remain within the contact to form a debris bed, plotted as a function of contact conformity and fretting frequency. Superimposed on the map are arrows representing changes in fundamental parameters which control debris retention (the temperature of the contact and the geometry of the contact) and the way that these depend upon the parameters upon which the map is constructed.

fretting wear scar was deemed indicative of oxygen exclusion from that region. Opening of the contact once per fretting cycle (by removal of the normal load) resulted in a change of the debris from nitride to the more thermodynamically favoured oxide.

(c) Mapping of the critical characteristics of debris type and debris retention in the fretting contact

The preceding discussion has focussed on two main processes which govern the nature of the fretting contact (and thus influence the mechanisms and rate of wear), namely the formation (or otherwise) of oxide debris within the contact, and the retention (or otherwise) of any debris formed within the contact. Accordingly, two fretting maps have been constructed to more clearly describe the influences of fretting frequency and contact geometry on these processes (based upon the observations for the steel-on-steel contact examined in this work), and to summarise the understanding of the factors which control the observed behaviour.

Fig. 15 describes regimes of behaviour in terms of the *debris type*, i.e. whether the debris is primarily oxide or metallic, summarising the observations that the debris was predominantly oxide, except in the case of a more-conforming contact fretting at high frequency, where a metallic debris resulted. Superimposed upon the map are two arrows which describe the physical processes which control the observed behaviour as follows: (a) a decrease in conformity of the contact enhances oxygen penetration from the atmosphere into all areas of the contact, since the decreased conformity results in reduction in the physical exclusion of the atmosphere due to the smaller distances over which penetration has to occur; (b) a decrease in fretting frequency results in a longer time between asperity contacts for the atmospheric oxygen to diffuse into the contact. Considering both of these, it is clear that only when the penetration of atmospheric oxygen is made difficult by both frequency effects and geometry effects does a primarily metallic debris result.

Secondly, Fig. 16 describes regimes of behaviour in terms of *debris retention* within the contact, summarising the observations that the debris formed is generally retained in the contact except when the contact geometry is less-conforming and the fretting frequency is low, where the debris

is observed to be lost from the contact. Superimposed upon the map are two arrows which describe the physical processes which control the observed behaviour as follows: (a) an increase in conformity of the contact results in more physical entrapment of the debris within the contact (also postulated by [7, 17]), since debris has further to travel to escape the contact; (b) an increase in fretting frequency results in a higher temperature being developed in the contact, which results in retention of oxide debris within the contact by softening of the underlying metal (leading to mechanical keying of the debris) and by promotion of sintering of the oxide debris particles themselves. Considering both of these, it is clear that only when both the physical entrapment of debris within the contact is low and the fretting frequency is low (leading to a low contact temperature) is the debris readily removed from the contact.

5. Conclusions

Within this work, it has been established that under certain circumstances, fretting frequency strongly influences fretting wear behaviour and thus wear rate. The influence of frequency is found to be dependent on the contact geometry; for less-conforming contacts, wear rate is significantly influenced by fretting frequency, with the wear rate under a fretting frequency of 200 Hz being $\sim$50 % of that observed in tests conducted with a fretting frequency of 5 Hz. With more-conforming contacts, the change in wear rate with fretting frequency is much less significant.

Changes in wear behaviour result from changes in the type of debris formed, and changes in the retention of debris within the contact once it has formed. Debris type is influenced by frequency and contact geometry via the control of oxygen penetration into the contact. Frequency controls the *time* that oxygen has to penetrate and react with the nascent metal surfaces which result from asperity interactions, with the result that at lower fretting frequencies, the debris is more likely to be in the form of an oxide. Contact conformity influences the *distance* over which the oxygen has to move to fully penetrate the contact, resulting in more-conforming contacts having a higher tendency to form metallic debris. Fretting frequency and contact geometry also influence the retention of debris which has formed within the fretting contact. Fretting frequency influences the contact *temperature*; at higher frequencies (and thus higher contact temperatures), any debris which has formed is more likely to coalesce (through sintering) and adhere to the contact (via softening and mechanical keying into the underlying metal) and thus debris retention is promoted. In addition, contact conformity provides a *physical barrier* to debris egress from the contact, associated with the longer distances over which the debris has to travel to escape.

Maps describing both the type of debris formed and the tendency for the debris to be retained in the contact as a function of the fretting frequency and contact conformity have been developed. The underlying physical processes which govern the behaviour have been superimposed upon these maps as a means of understanding the observations within a physically coherent framework.

Acknowledgements

The authors wish to thank Rolls-Royce plc, Aerospace Group for their financial support of the research, which was carried out at the University Technology Centre in Gas Turbine Transmission Systems at the University of Nottingham. In addition, the authors wish to thank the Taiho Kogyo Tribology Research Foundation, Toyota City, Japan for supporting an upgrade of the experimental facilities which have underpinned this work. The views expressed in this paper are those of the authors and not necessarily those of Rolls-Royce plc, Aerospace Group or Taiho Kogyo Tribology Research Foundation.

References

1 O. Vingsbo, S. Soderberg, On fretting maps, Wear 126 (1988) 131–147.
2 J. M. Dobromirski, Variables of fretting process: are there 50 of them, Standardization of Fretting Fatigue Test Methods and Equipment 1159 (1992) 60–66.

3 Y. Berthier, L. Vincent, M. Godet, Velocity accommodation in fretting, Wear 125 (1988) 25–38.
4 J. Ding, I. R. McColl, S. B. Leen, P. H. Shipway, A finite element based approach to simulating the effects of debris on fretting wear, Wear 263 (2007) 481–491.
5 J. Ding, S. B. Leen, E. J. Williams, P. H. Shipway, A multi-scale model for fretting wear with oxidation-debris effects, Proceedings of the Institution of Mechanical Engineers, Part J: Journal of Engineering Tribology 223 (2009) 1019–1031.
6 B. Van Peteghem, S. Fouvry, J. Petit, Effect of variable normal force and frequency on fretting wear response of Ti-6Al-4V contact, Wear 271 (2011) 1535–1542.
7 S. Fouvry, C. Paulin, S. Deyber, Impact of contact size and complex gross partial slip conditions on Ti6Al4V/Ti6Al4V fretting wear, Tribology International 42 (2009) 461–474.
8 S. Soderberg, U. Bryggman, T. McCullough, Frequency effects in fretting wear, Wear 110 (1986) 19–34.
9 A. Ramalho, J. P. Celis, Fretting Laboratory Tests: Analysis of the Mechanical Response of Test Rigs, Tribology Letters 14 (2003) 187–196.
10 I.-M. Feng, H. H. Uhlig, Fretting corrosion of mild steel in air and in nitrogen, Journal of Applied Mechanics-Transactions of the Asme 21 (1954) 395–400.
11 H. H. Uhlig, Mechanism of fretting corrosion, Journal of Applied Mechanics-Transactions of the Asme (1954) 401–407.
12 L. Toth, The investigation of the steady stage of steel fretting, Wear 20 (1972) 277–286.
13 G. H. G. Vaessen, C. P. L. Commissaris, A. W. J. Gee, Fretting corrosion of Cu-Ni-Al against plain carbon steel, Proceedings of the Instatution of Mechanical Engineers 183 (1968) 125–128.
14 U. Bryggman, S. Söderberg, Contact conditions in fretting, Wear 110 (1986) 1–17.
15 M. Odfalk, O. Vingsbo, Influence of normal force and frequency in fretting, Tribology transactions 33 (1990) 604–610.
16 I. R. McColl, J. Ding, S. B. Leen, Finite element simulation and experimental validation of fretting wear, Wear 256 (2004) 1114–1127.
17 R. Merhej, S. Fouvry, Contact size effect on fretting wear behaviour: application to an AISI 52100/AISI 52100 interface, Lubrication Science 21 (2009) 83–102.
18 A. R. Warmuth, S. R. Pearson, P. H. Shipway, W. Sun, The effect of contact geometry on fretting wear rates and mechanisms for a high strength steel, Wear 301 (2013) 491–500.
19 S. Fouvry, R. Merhej, Introduction of a power law formulation to quantify the contact size effects on friction and wear responses of dry oscillating sliding contacts: Application to a chromium steel interface, Wear 301 (2013) 34–46.
20 C. Mary, S. Fouvry, J. M. Martin, B. Bonnet, Pressure and temperature effects on fretting wear damage of a Cu-Ni-In plasma coating versus Ti17 titanium alloy contact, Wear 272 (2011) 18–37.
21 A. L. Mohd Tobi, J. Ding, S. R. Pearson, S. B. Leen, P. H. Shipway, The effect of gross sliding fretting wear on stress distributions in thin W-DLC coating systems, Tribology International 43 (2010) 1917–1932.
22 S. Fouvry, P. Duó, P. Perruchaut, A quantitative approach of Ti-6Al-4V fretting damage: friction, wear and crack nucleation, Wear 257 (2004) 916–929.
23 K. Elleuch, S. Fouvry, Wear analysis of A357 aluminium alloy under fretting, Wear 253 (2002) 662–672.
24 N. Birks, G. H. Meier, F. S. Pettit, Introduction to the High Temperature Oxidation of Metals, Cambridge University Press, 2006.
25 K. Schouterden, B. Blanpain, J. P. Celis, O. Vingsbo, Fretting of titanium nitride and diamond-like carbon coatings at high frequencies and low amplitude, Wear 181-183 (1995) 86–93.
26 S. R. Pearson, P. H. Shipway, J. O. Abere, R. A. A. Hewitt, The effect of temperature on wear and friction of a high strength steel in fretting, Wear 303 (2013) 622–631.
27 Bill R. C., Review of the factors that influence fretting wear, ASTM STP 780, American Society for Testing and Materials, 1982.
28 C. Herring, Effect of change of scale on sintering phenomena, Journal of Applied Physics 21 (1950) 301–303.
29 B. D. Leonard, A. Ghosh, F. Sadeghi, S. Shinde, M. Mittelbach, Third body modeling in fretting using the combined finite-discrete element method, International Journal of Solids and Structures 51 (2014) 1375–1389.